



Structural exploration of selected C6 and C7-substituted coumarin isomers as selective MAO-B inhibitors

Yassir Boulaamane, Iqrar Ahmad, Harun Patel, Niloy Das, Mohammed Reda Britel & Amal Maurady

To cite this article: Yassir Boulaamane, Iqrar Ahmad, Harun Patel, Niloy Das, Mohammed Reda Britel & Amal Maurady (2022): Structural exploration of selected C6 and C7-substituted coumarin isomers as selective MAO-B inhibitors, *Journal of Biomolecular Structure and Dynamics*, DOI: [10.1080/07391102.2022.2033643](https://doi.org/10.1080/07391102.2022.2033643)

To link to this article: <https://doi.org/10.1080/07391102.2022.2033643>



Published online: 15 Feb 2022.



Submit your article to this journal



Article views: 109



View related articles



CrossMark

View Crossmark data

RESEARCH ARTICLE



Structural exploration of selected C6 and C7-substituted coumarin isomers as selective MAO-B inhibitors

Yassir Boulaamane^a , Iqrar Ahmad^b , Harun Patel^b , Niloy Das^c , Mohammed Reda Britel^a and Amal Maurady^{a,d}

^aLaboratory of Innovative Technologies, National School of Applied Sciences of Tangier, Abdelmalek Essaadi University, Tetouan, Morocco;

^bDivision of Computer Aided Drug Design, Department of Pharmaceutical Chemistry, R. C. Patel Institute of Pharmaceutical Education and Research, Shirpur, India; ^cDepartment of Pharmacy, BGC Trust University Bangladesh, Chittagong, Bangladesh; ^dLaboratory of Innovative Technologies, Faculty of Sciences and Techniques of Tangier, Abdelmalek Essaadi University, Tetouan, Morocco

Communicated by Ramaswamy H. Sarma

ABSTRACT

Monoamine Oxidase B is considered a successful target for developing antiparkinsonian drugs. Due to the side effects of current MAO-B inhibitors, there's an urgent need for novel potent and highly selective MAO-B inhibitors. A recent study has shown that coumarins tend to be more selective towards MAO-B than MAO-A when connected to a hex-5-ynyl chain at position 6 in contrast to their C7-isomers. The present study describes the mode of interaction of the C6 and C7-substituted coumarin isomers characterized by their difference in selectivity towards MAO-B through molecular docking and molecular dynamics simulations in an effort to elucidate the structural components and molecular interactions that may be responsible for MAO-B selectivity. Three isomeric coumarin pairs connected to ether chain at position 6 or 7 were taken from the literature and modelled according to their IUPAC nomenclature. Molecular docking study revealed one π - π stacking interaction with Tyr-326 in common between the selective coumarin C6-isomers. Resulting complexes of one isomeric coumarin pair that displayed the highest selectivity shift towards MAO-B were subject to 100 ns molecular dynamics simulations study to analyze the stability of the docked complexes. Molecular dynamics revealed that the C7-isomer is relatively stable in both MAO isoforms through the simulation duration, whereas the C6-isomer deemed unstable for MAO-A which may be due to the bulky Phe-208 residue in MAO-A. Our results might be applied for further development and optimization of coumarin derivatives into a successful drug against Parkinson's disease.

ARTICLE HISTORY

Received 12 August 2021
Accepted 10 January 2022

KEYWORDS

Coumarin; selectivity; monoamine oxidase A; monoamine oxidase B; molecular docking; Parkinson's disease; ADME; drug likeness; Lipinski's rule of five; molecular dynamics simulation

1. Introduction

Parkinson's disease (PD) is a neurodegenerative disorder defined by the progressive loss of dopaminergic neurons in the substantia nigra pars compacta (SNpc) of the mid brain (Noda et al., 2020). It is estimated to affect 6 million people worldwide with a prevalence of 150 in every 100 000 people which is expected to further increase by 2- to 3-fold until 2030 (Poewe & Mahrknecht, 2020). It is considered the second most frequent neurodegenerative disorder after Alzheimer's disease (Dorsey et al., 2018). Current available drugs for treating PD include levodopa, which remains the most used therapy, dopamine agonists and catechol-O-methyl transferase (COMT)/monoamine oxidase (MAO) inhibitors (Youdim et al., 2006). Monoamine Oxidase (MAO) (EC 1.4.3.4) is a flavoenzyme attached to the outer mitochondrial membrane of the neurons, it is responsible for the oxidative deamination of monoamine neurotransmitters such as dopamine, adrenaline and noradrenaline in the central nervous system (CNS) (Shih et al., 1999). The MAO enzyme exists in two forms namely MAO-A and MAO-B that share about 70%

of their amino acid identity, but differ in their tissue distribution, substrate and inhibitor preferences (Youdim et al., 2006). Development of the first MAO inhibitors was abandoned since the discovery that their use potentiates a 'cheese effect' related to the metabolism of tyramine, which causes a cardiovascular crisis (Culpepper, 2013; Youdim et al., 2006). However, a new class of selective MAO-B inhibitors has proven to be efficient in treating PD symptoms. It was also shown that this new class of MAO inhibitors are devoid of the tyramine related side effects. Furthermore, they may act as neuroprotective agents by limiting the release of free radical species and hence may decrease the progression of the disease (Tetrud & Koller, 2004; Youdim et al., 2006).

MAO-A has serotonin as its preferred substrate while MAO-B preferentially deaminates 2-phenylethylamine and benzylamine. Dopamine, norepinephrine, and epinephrine are metabolized by both isoforms in most animal tissues (Finberg & Rabey, 2016).

During aging, the expression of MAO-B increases in the brain and is connected with an enhanced dopamine metabolism that produce reactive oxygen species (ROS) such as

hydrogen peroxide (H_2O_2) resulting in oxidative damage and apoptotic signaling events (Mallajosyula et al., 2008).

Previously approved MAO-B inhibitors are selegiline and rasagiline which irreversibly inhibits MAO-B with an IC_{50} value of 6.8 nM and 14 nM respectively (Youdim et al., 2001). The latest approved MAO-B inhibitor was safinamide which reversibly inhibits MAO-B with an IC_{50} value of 450 nM and a selectivity index ($\text{SI} = \text{IC}_{50} \text{ MAO-A}/\text{IC}_{50} \text{ MAO-B}$) of over 700 (Binda et al., 2007).

Crystal structure of MAO-A has a monopartite substrate cavity of $\sim 550 \text{ \AA}^3$ volume while crystal structure of MAO-B contains a dipartite cavity structure with an entrance cavity of $\sim 290 \text{ \AA}^3$ and a substrate cavity of $\sim 400 \text{ \AA}^3$ (De Colibus et al., 2005). Ile-199 and Tyr-326 side chains separate these two cavities in MAO-B (Binda et al., 2003). Mutagenesis studies of mutant Ile-199Phe in MAO-B show that the bulky side chain of Phenylalanine limits conformational flexibility of this residue in MAO-B, and hence prevents larger cavity-spanning inhibitors from binding to both cavities (Mostert et al., 2015). The smaller side chain of Ile-199 is more flexible and may exhibit conformational changes to merge both cavities and allow the binding of larger inhibitors. Tyr-326 is also another key residue that plays a role in the selectivity mechanism of MAO-B, the bulky side chain of this residue restricts the binding of certain inhibitors such as harmine (Mostert et al., 2015). The corresponding residue in MAO-A is Ile-335, which is smaller and allows the binding of harmine. Thus, Ile-199 and Tyr-326 serves as 'gating' residues and a structural determinant for substrate and inhibitor recognition by MAO-B (Edmondson et al., 2007). MAO-A and MAO-B structures and active site cavities are shown in Figure 1.

Structural study revealed that MAO-B (PDB ID: 2V61) is formed by two monomers consisting of a globular domain anchored to the membrane through a C-terminal helix (Binda et al., 2002). The active site is located in the substrate fixing domain located near the FAD cofactor binding domain and is formed by the residues: Tyr-60, Pro-102, Pro-104, Leu-164, Phe-168, Leu-171, Cys-172, Ile-198, Ile-199, Gln-206, Ile-316, Tyr-326, Phe-343, Tyr-398 and Tyr-435 (Binda et al., 2007). Meanwhile, MAO-A (PDB ID: 2Z5Y) is expressed as a monomer consisting of a C-terminal domain that forms helical tails which are responsible for attaching the protein to the membrane. Structural analysis revealed that the active site of MAO-A is located in the substrate cavity near the FAD cofactor cavity and is formed by the residues: Tyr-69, Asn-181, Phe-208, Val-210, Gln-215, Cys-323, Ile-325, Ile-335, Leu-337, Phe-352, Tyr-407, Tyr-444 (Binda et al., 2011).

Coumarin is a highly flexible scaffold that has been extensively studied for developing new MAO inhibitors displaying a wide range of selectivity for MAO-B (Rempel et al., 2012). In a previous study conducted by Mertens et al. (2014), it was reported that alkynyl coumarinyl ethers are able to inhibit MAO-B at nanomolar concentrations ranging from 0.58 nM to 1790 nM with a selectivity for MAO-B reaching a value of over 3400-fold (Mertens et al., 2014). The compounds were found to be reversible inhibitors and it was concluded that the triple bond doesn't form a covalent bond

with the propargyl group as noted in the irreversible inhibitors, selegiline and rasagiline (Mertens et al., 2014).

In an effort to develop new potent and highly selective MAO-B inhibitors, we used molecular modelling techniques to get an insight on the possible molecular mechanisms of three isomeric coumarin pairs in which the inhibitory activity and selectivity for MAO-B were previously evaluated *in vitro* (Mertens et al., 2014).

Molecular docking study was carried out to investigate the structural conformations of these compounds with crystallographic structures of MAO-A and MAO-B and to identify key interactions that may enhance the selectivity for MAO-B. Furthermore, *in silico* ADME properties were evaluated in order to evaluate the drug likeness of the selected compounds.

Finally, two isomeric coumarins that displayed the highest selectivity shift towards MAO-B were subject to 100 ns molecular dynamics in order to compare their stability over time and to investigate the key residues that are involved during the protein-ligand interaction.

2. Materials and methods

2.1. Preparation of the target proteins

Crystallographic structures of human MAO-A were fetched from the RCSB Protein Data Bank (<http://www.rcsb.org/>) and the structure with the highest resolution (PDB ID: 2Z5Y, resolution = 2.1 Å) bound to a known inhibitor, harmine (HRM) was selected (Son et al., 2008). MAO-B structure bound to a coumarin derivative, 7-(3- chlorobenzyloxy)-4-(methylamino) methyl-coumarin (C18) with the highest resolution was chosen (PDB ID: 2V61, resolution = 1.7 Å), the co-crystallized coumarin scaffold in this structure was used to superimpose docked ligands and choose the most similar binding pose to the native ligand (Binda et al., 2007). Co-crystallized ligands and water molecules were removed as they weren't involved in the ligand binding, they were therefore deleted to make computations easier and clear the binding pocket of possible water molecules that would distort the pose search (Wang et al., 2019). FAD cofactor was kept as it plays an important role in the proper functioning of the enzyme in catalyzing the deamination of monoamines and to investigate whether it's involved in ligand binding to the protein during the molecular docking study (Gaweska & Fitzpatrick, 2011). Protein preparation wizard (PPW) in Maestro 12.5 was used to assign bond orders, adding explicit hydrogens to the structure, fixing and optimizing side chains missing atoms using Prime (Schrödinger Release: Maestro, 2021; Jacobson et al., 2004; Jacobson et al., 2002; Greenwood et al., 2010). Protonation states for the residues were assigned using PROPKA program for predicting the pK_a of protein residues at $\text{pH} = 7.0$ (Olsson et al., 2011). The bound native ligands were used to define the active site residues of the target proteins.

2.2. Preparation of ligands

Selected coumarin isomers were retrieved from Mertens et al. (2014) experimental study and converted to chemical structures from their IUPAC nomenclature using 2D Sketcher

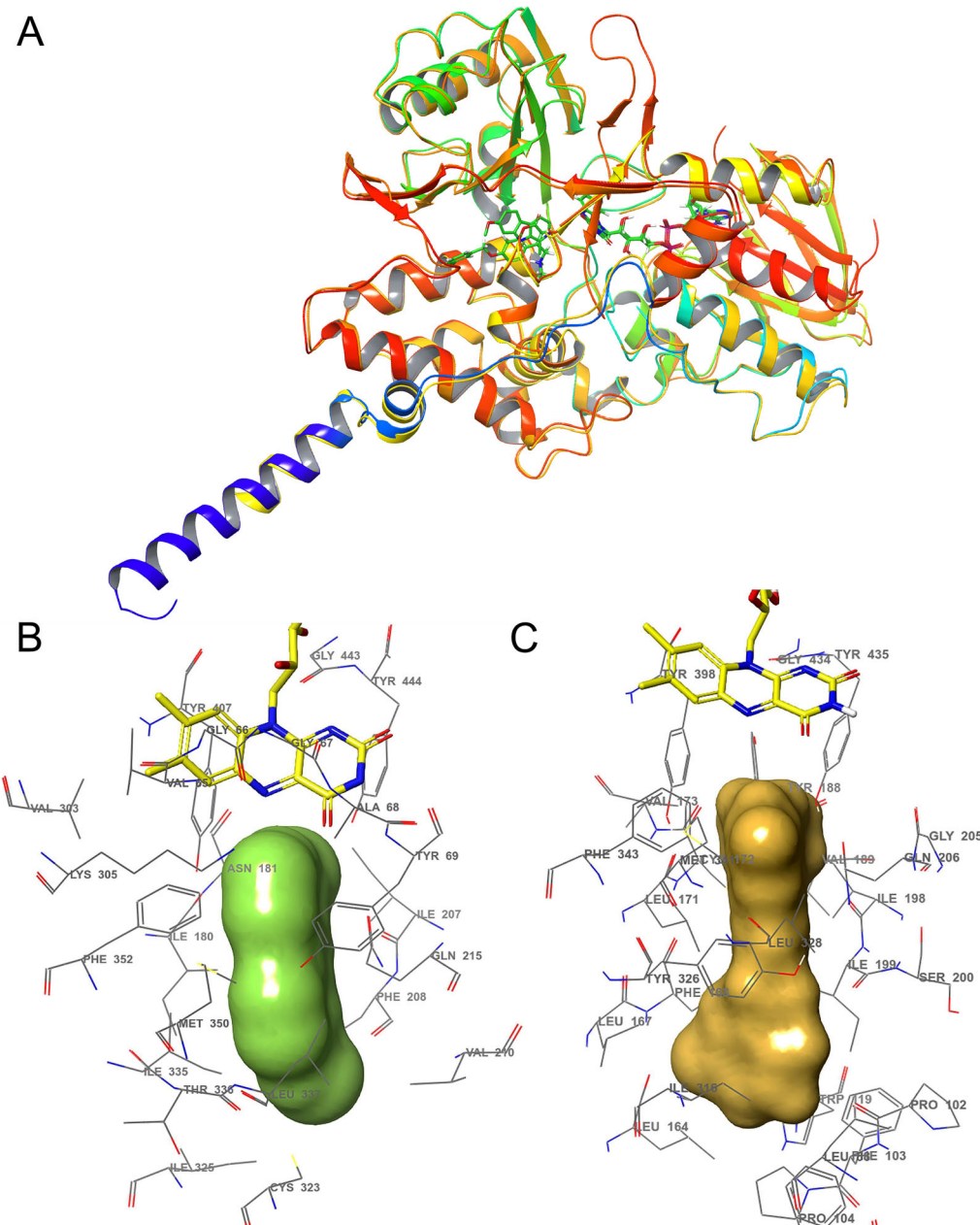


Figure 1. Superposition of crystal structures of MAO-A (PDB ID: 2Z5Y) and MAO-B (PDB ID: 2V61) (A). Binding surfaces and active site residues of MAO-A (B) and MAO-B (C).

module included in Maestro 12.5 (Mertens et al., 2014; Schrödinger Release: Maestro, 2021). Explicit hydrogens and 3D coordinates were also generated. Ligprep module was used for energy minimization using Optimized Potentials for Liquid Simulations (OPLS3e) force field, ionization states and other parameters were kept unchanged (Roos et al., 2019). Chemical structures of coumarin isomers and their respective MAO-B selectivity are reported in Table 1.

2.3. Molecular docking study and binding free energy calculations

Molecular docking was used for analysis of interactions between the coumarin isomers and the active site of MAO-B and MAO-A. Ligand docking was performed by employing Glide program in Maestro 12.5 (Schrödinger Release: Maestro,

2021). Co-crystallized ligands were used for grid box placing with a spacing of 1 Å using receptor grid generation tool of Maestro 12.5 (Schrödinger Release: Maestro, 2021). Grid dimensions were chosen large enough ($24 \times 24 \times 24$ Å) in x, y and z directions, respectively, to fit the following amino acids of the active sites of the proteins: Tyr-60, Pro-102, Pro-104, Leu-164, Phe-168, Leu-171, Cys-172, Ile-198, Ile-199, Gln-206, Ile-316, Tyr-326, Phe-343, Tyr-398 and Tyr-435 for MAO-B and Tyr-69, Asn-181, Phe-208, Val-210, Gln-215, Cys-323, Ile-325, Ile-335, Leu-337, Phe-352, Tyr-407, Tyr-444 for MAO-A. The grid box was positioned in a way to cover the entire binding site and to allow larger molecules to dock properly ($51.2 \times 155.5 \times 28.7$ Å for MAO-B and $-40.6 \times -26.7 \times -14.9$ Å for MAO-A) in x, y and z directions, respectively. Ligand docking was performed using Glide Extra Precision (XP) mode included in Maestro 12.5 (Friesner et al., 2006; Halgren et al., 2004; Schrödinger Release:

Table 1. Chemical structures of coumarin isomers and their MAO-B selectivity [20].

Compound	Nomenclature	Chemical structure	SI
1	Methyl 2-oxo-7-(hex-5-ynyloxy)-2H-chromene-3-carboxylate		6.8
2	Methyl 6-(hex-5-ynyloxy)-2-oxo-2H-chromene-3-carboxylate		81.3
3	Methyl 7-(4-chlorophenoxy)-2-oxo-2H-chromene-3-carboxylate		53
4	Methyl 6-(4-chlorophenoxy)-2-oxo-2H-chromene-3-carboxylate		>83.3
5	N-(2-Oxo-7-(hex-5-ynyloxy)-2H-chromen-3-yl) acetamide		1.6
6	N-(2-Oxo-6-(hex-5-ynyloxy)-2H-chromen-3-yl) acetamide		>404.8

SI: Selectivity index (IC_{50} MAO-A/ IC_{50} MAO-B).

Maestro, 2021). Conformations of docked ligands were chosen according to their binding energy and their conformation similarity to the native ligands. Finally, binding free energy calculations were performed by employing Prime MM-GBSA approach using Variable Dielectric Surface Generalized Born (VSGB) as an implicit solvent model and OPLS3e force field for the resulting protein-ligand complexes to estimate ligand-binding affinities (Genheden & Ryde, 2015; Li et al., 2011). The values were calculated based on the following equation (Das et al., 2009; Lyne et al., 2006):

$$\Delta G_{bind} = \Delta E_{mm} + \Delta G_{solv} + \Delta G_{sa}$$

$$\Delta E_{mm} = E_{complex} - (E_{protein} + E_{ligand})$$

Where, ΔE_{mm} is the difference in the minimized energies between the obtained protein-ligand complexes and the sum of the protein and ligand energies individually. ΔG_{solv} is the difference in the GBSA solvation energy of the protein-ligand complex and the sum of the solvation energies of protein and ligand in the unbound state. ΔG_{sa} is the difference between the surface area energies for the complex and the sum of the surface area energies for the free protein and ligand.

$E_{complex}$, $E_{protein}$, and E_{ligand} are the minimized energies of the protein-ligand complex, free protein, and ligand, respectively.

2.4. ADME properties prediction

It has been estimated that nearly 40% of drug candidates fail in clinical trials due to poor Absorption, Distribution, Metabolism and Excretion (ADME) properties (Lin et al., 2003). *In silico* ADME prediction is a cost-efficient approach to find if a compound is druglike by calculating its pharmacokinetics parameters and physicochemical properties and can considerably reduce the amount of consumed time and resources during the overall drug development process. The selected compounds were analyzed based on Lipinski's' Rule of Five' which allows the evaluation of physicochemical properties that would make it likely for a drug to be orally active in humans (Congreve et al., 2003; Lipinski, 2004). Pharmacokinetic parameters including water solubility, human oral absorption, blood-brain barrier permeability, human colon adenocarcinoma (Caco-2) and Madin-Darby Canine Kidney (MDCK) cell permeability were predicted using Qikprop tool in Maestro 12.5 (Schrödinger Release: Maestro, 2021).

2.5. Molecular dynamics simulation

Two coumarin isomers **5** and **6** characterized by their highest selectivity shift towards MAO-B in complex with MAO-A and MAO-B were taken from the molecular docking study. The

docked complexes were prepared using the protein preparation wizard (PPW) in Maestro 12.5 in order to fix structural defects. Non-standard residues such as FAD cofactor were removed because they weren't directly involved in the ligand binding to crystal structures of MAO-B (PDB ID: 2V61) and MAO-A (PDB ID: 2Z5Y) despite its catalytic role in the proper functioning of the protein (Binda et al., 2007; Son et al., 2008). Moreover, the FAD cofactor didn't display any type of interaction with coumarin derivatives during the molecular docking study, therefore we removed FAD cofactor from MD simulation study. Missing side chains and loops were fixed using Prime. Desmond module was used to run a MD simulation to investigate the change in protein structure within the solvent system (D. E. Shaw Research, Schrödinger Release, 2020–3). The water-soaked solvated system was created in Desmond using the System Builder panel. For the simulations, the complex was centered in an orthorhombic cubic box with periodic boundary conditions and filled with Single Point Charge (SPC) water molecules buffered at a distance of minimum 10 Å between a protein atom and box edges (Ahmad et al., 2021; Zrieq et al., 2021). The system was neutralized by randomly adding a sufficient number of counter-ions (Na^+ and Cl^-) and isosmotic state was maintained by adding 0.15 M NaCl. Then, the solvated built system was minimized and relaxed utilizing OPLS3e force field parameters as the default protocol associated with Desmond (Jorgensen et al., 1996; Pawara et al., 2021). A constant 300 K temperature and 1 atm pressure was maintained during the simulation using the Nose-Hoover thermostat algorithm and Martyna-Tobias-Klein Barostat algorithm, respectively (Mehta et al., 2019). A total of 100 ns simulations were conducted, during which 1000 trajectories were saved. Lastly, MD simulation trajectory was analyzed using the Simulation Interaction Diagram (SID) tool (Lee et al., 2021; Martyna, 1994).

3. Results

3.1. Validation of the docking protocol

The docking protocol implemented in Glide module was validated by redocking the crystal ligands of human MAO-B (PDB ID: 2V61) and MAO-A (PDB ID: 2Z5Y). Co-crystallized ligands were modelled using 2D Sketcher module included

in Maestro 12.5, explicit hydrogens and 3D coordinates were generated, Ligprep was employed for energy minimization using default settings (Gaweska & Fitzpatrick, 2011). The root-mean-square deviation (RMSD) was calculated by superimposing both docked and native ligands, the later was used as a reference. The results yielded values of 1.81 Å for MAO-B and 1.47 Å for MAO-A which indicates a good accuracy of the docking program (Figure 2).

3.2. Molecular docking of coumarin isomers with MAO-B and MAO-A

Molecular docking study was performed using Glide module included in Maestro 12.5 with extra precision (XP) mode (Friesner et al., 2004; 2006; Halgren et al., 2004; Wang et al., 2019). Conformations of docked compounds were ranked by their energies and then selected based on their similarity to the co-crystallized ligands by mean of superposition.

Hydrogen bonds and nearby interacting hydrophobic amino acids were identified using Ligand interaction diagram of Maestro 12.5 (Schrödinger Release: Maestro, 2021). Molecular docking results of coumarin isomers with MAO-B and MAO-A and MM-GBSA binding free energy of the resulting protein-ligand complexes are shown in Table 2 and Table 3 respectively. Protein-ligand interactions diagrams of the selected ligands with MAO-B and MAO-A are shown in Figures 3 and 4 respectively.

Molecular docking study revealed that coumarin derivatives and their isomers bind more optimally within MAO-B active site than MAO-A active site regardless of their selectivity. The docking scores of Glide XP mode varied from -8.96 to -10.47 kcal/mol for MAO-B. The compound 3 which displayed the lowest binding energy (-10.47 kcal/mol) is considered the most potent MAO-B inhibitor among the selected coumarin derivatives which is in correlation with the experimental study ($\text{IC}_{50} = 1.41 \text{ nM}$) (Mertens et al., 2014).

Structural analysis demonstrated that all coumarin derivatives bind to MAO-B with the coumarin scaffold directed towards the aromatic cage consisting of Tyr-398, Tyr-435 and FAD-1502. Compound **2**, **4** and **5** established a hydrogen bond with the aromatic residue Tyr-188 which is located at the

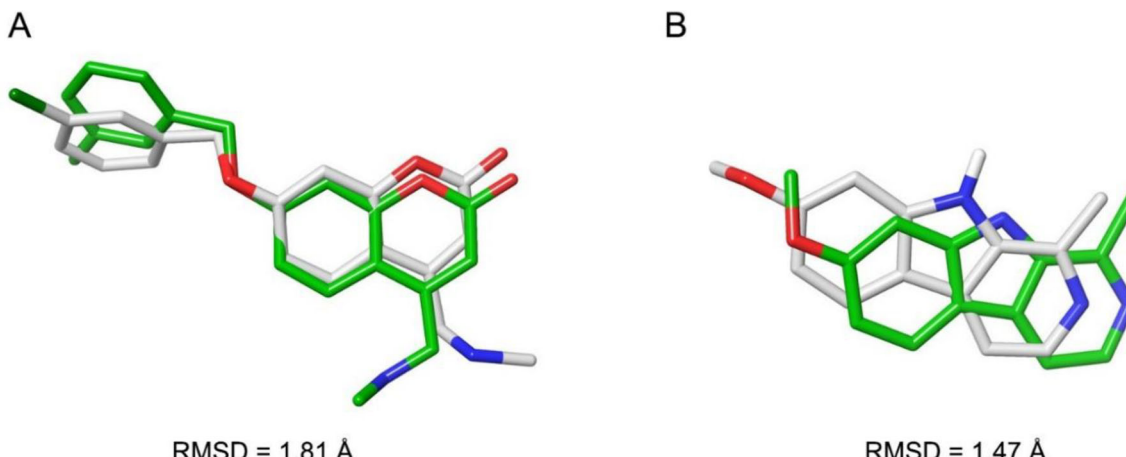


Figure 2. RMSD values and superimposition of native co-crystallized and docked ligands for MAO-B (A) and MAO-A (B).

Table 2. Docking results and MM-GBSA binding free energy of the selected ligands with MAO-B.

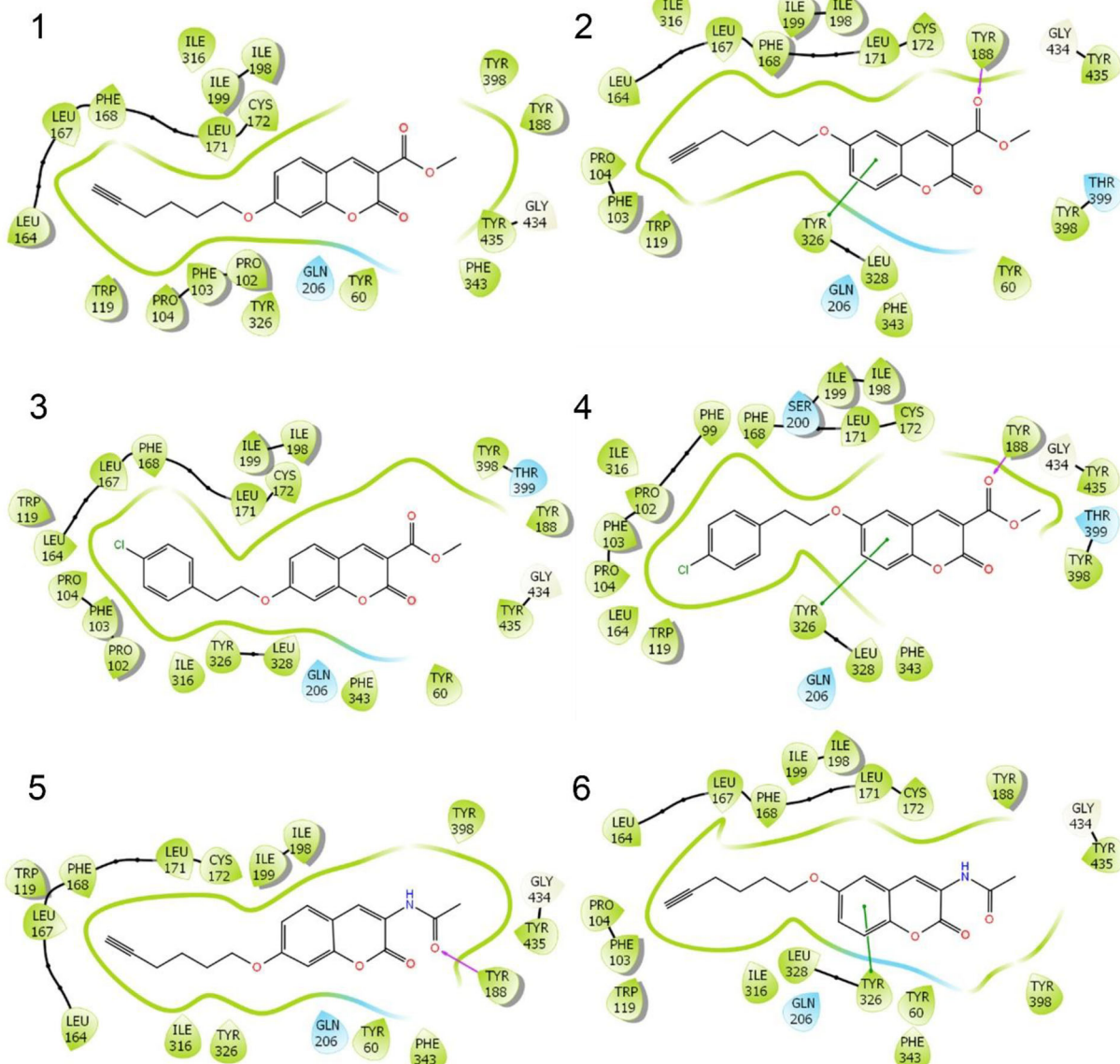
Compound	Glide XP score (kcal/mol)	MM-GBSA binding free energy (kcal/mol)
1	-10.22	-66.47
2	-9.24	-64.18
3	-10.47	-69.83
4	-8.96	-54.75
5	-9.45	-54.70
6	-9.76	-45.23

bottom of the substrate cavity. This residue may play a role in anchoring inhibitors within MAO-B active site and thus increasing their stability. However, this residue doesn't seem to be involved in the MAO-B selectivity mechanism as it is not interacting with the most selective coumarin isomer (**6**). On the other hand, the comparison of the C6-substituted coumarin isomers has revealed a common interaction between those compounds which is a π - π stacking interaction between the coumarin ring and the gating residue Tyr-326. This residue is replaced by the aliphatic amino acid Ile-335 in MAO-A and thus

Table 3. Docking results and MM-GBSA binding free energy of the selected ligands with MAO-A.

Compound	Glide XP score (kcal/mol)	MM-GBSA binding free energy (kcal/mol)
1	-7.93	-34.23
2	-4.97	-29.49
3	-4.14	-17.81
4	1.66	-52.60
5	-4.40	-41.60
6	-2.39	-35.32

might have a role in the selectivity of the selected coumarin isomers towards MAO-B. MM-GBSA binding free energy calculations were performed in order to assess the ligand-binding affinities, the results show that the C6-substituted coumarin isomers in complex with MAO-B tend to be slightly less stable when compared to the C7-substituted coumarin isomers. We note that those results correlate well with the experimental data which demonstrated that C6-substituted coumarins are slightly less potent towards MAO-B regardless of their selectivity (Mertens et al., 2014).

**Figure 3.** Protein-ligand interactions of the selected ligands with MAO-B.

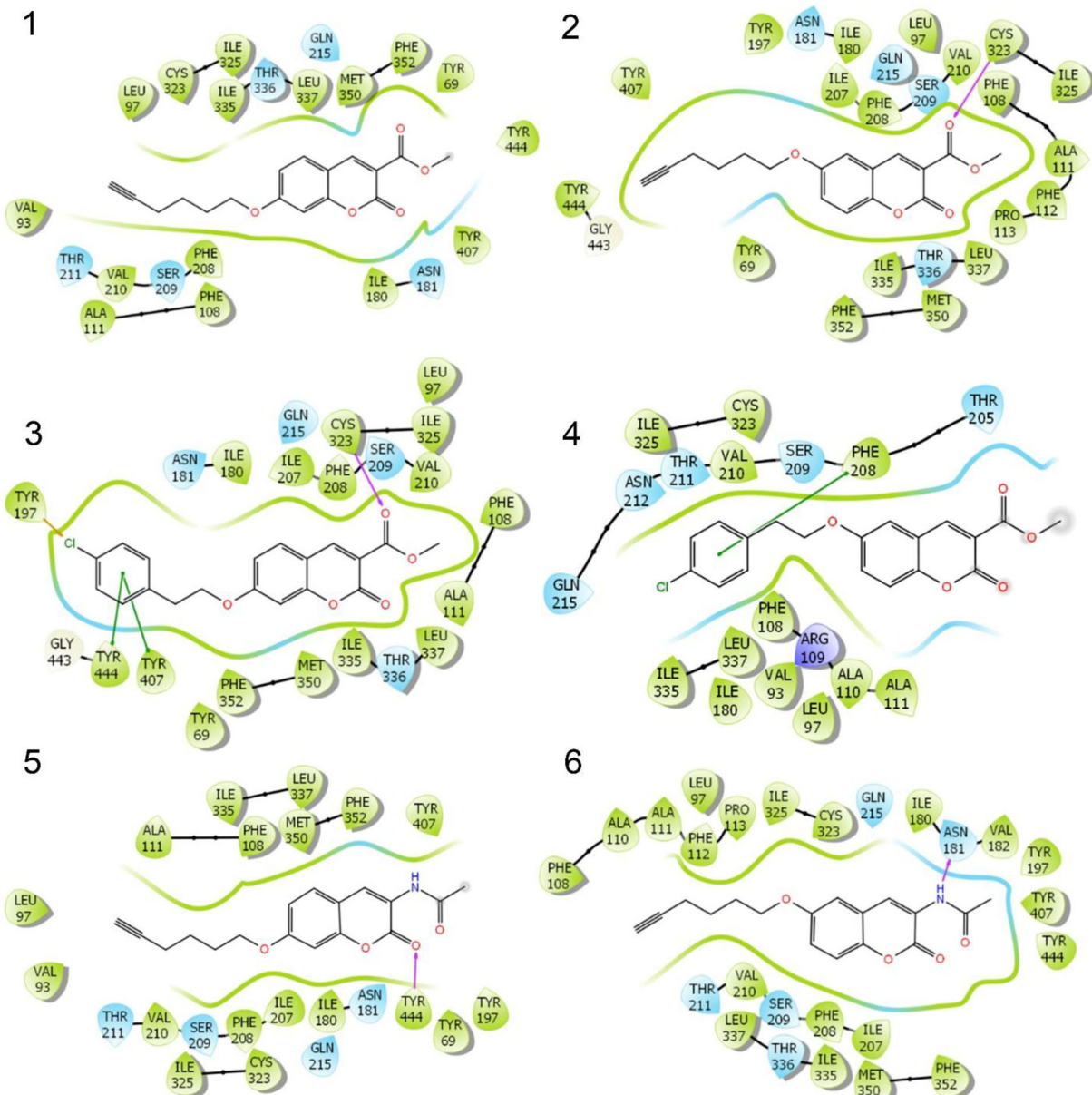


Figure 4. Protein-ligand interactions of the selected ligands with MAO-A.

Molecular docking study of coumarin derivatives and their isomers with MAO-A active site yielded docking scores ranging from 1.66 to -7.93 kcal/mol . The C6-substituted coumarin isomers are showing high binding scores compared to their C7-isomers, this is in accordance with the previously reported experimental data which demonstrated that the C6-isomers of coumarin derivatives tend to lose inhibitory activity for MAO-A (Mertens et al., 2014). MMGBSA binding free energy calculations showed relatively lower affinities when compared to coumarin isomers in complex with MAO-B.

Binding conformations of coumarin isomers with MAO-B and MAO-A are shown in Figures 5 and 6 respectively. Docking poses analysis show that all the compounds bind to MAO-B with the coumarin scaffold directed towards the

substrate cavity with either the hex-5-ynoate chain or the 4-chlorophenoxy moiety occupying the entrance cavity and forming various hydrophobic interactions with nearby residues such as Pro-102, Pro-103, Pro-104, Leu-164, Leu-167, Phe-168 and Leu-171. Docking analysis of coumarin isomers with MAO-A has yielded different poses due to the smaller cavity of MAO-A, the hex-5-ynoate chain doesn't fit well inside MAO-A cavity and thus adopt different conformations which are less stable than those of MAO-B complexes. Furthermore, the coumarin isomer (4) bearing the 4-chlorophenoxy at C6 doesn't seem to fit well inside the MAO-A active site pocket which might be due to the bulkier chlorophenyl ring, this result is in accordance with the experimental data ($\text{IC}_{50} \text{ MAO-A} > 10\,000\text{ nM}$) which further emphasize our hypothesis (Mertens et al., 2014).

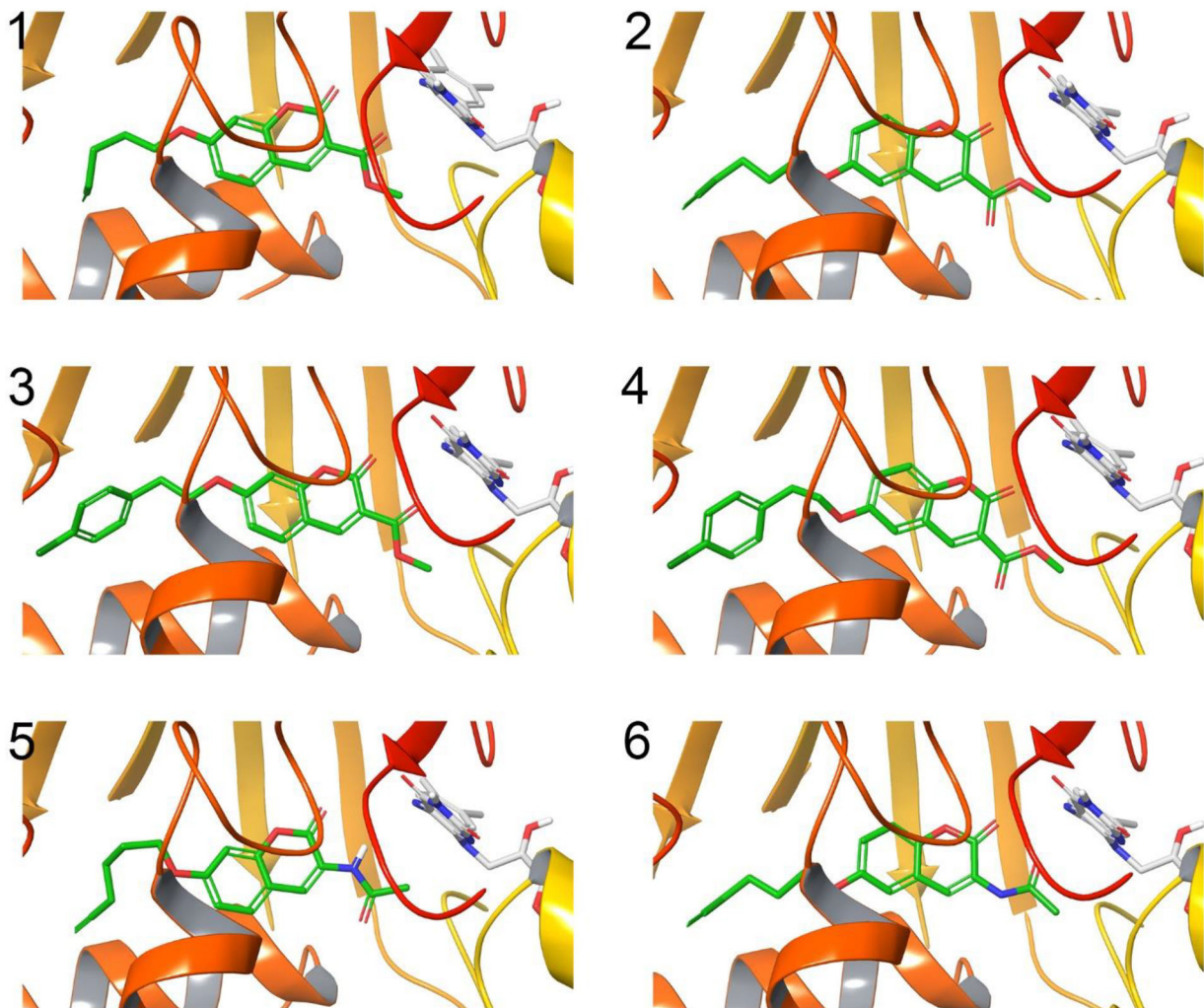


Figure 5. Docking poses of coumarin isomers with MAO-B active site. Binding conformations of coumarins are shown in green color, the C7-isomers are shown in 1,3,5 and their respective C6-isomers are shown in 2,4,6. FAD cofactor is shown in white color.

3.3. ADME properties prediction results

ADME properties and the ‘Rule of Five’ results for the selected coumarin isomers are shown in Table 4. All compounds were predicted as drug-like without any violations to the five rules. Qikprop predicted aqueous solubility show that all the compounds have values within the recommended range (-6.5 to 0.5) where 95% of similar values for known drugs fall inside. Predicted human oral absorption shows that all the selected coumarins have great oral absorption and thus greater bioavailability. Predicted apparent Caco-2 cell permeability yielded values greater than 500 which indicates a good cell permeability for the selected coumarins. Predicted brain/blood partition coefficient showed values greater than -3.0 and less than 1.2 which falls into the recommended range for drugs acting on the CNS. MDCK cells are considered to be a good mimic for the blood-brain barrier, predicted apparent MDCK cell permeability is considered great if >500 and poor if <25. The predicted MDCK values show that isomers 3 and 4 have great MDCK cell permeability, meanwhile it’s considered to be moderate for the other compounds.

3.4. Molecular dynamics analysis

Molecular dynamics simulation was carried out in order to enumerate the structural stability of MAO enzyme variants in the presence of C6- and C7- coumarin isomers, as this could give a first-hand clue into their perturbing effects on protein structural integrity (Figure 7).

a) Root-mean square deviation (RMSD)

The stability of the two coumarin isomers in complex with MAO-A and MAO-B was evaluated according to different parameters. Protein RMSD of C-alpha atoms was used to measure the conformational changes of given complexes over time and describes whether the simulation has equilibrated and if its fluctuations towards the end of the simulation are around some thermal average structure with respect to the initial structure obtained from the molecular docking study of 0 ns as a reference structure. For all the complexes, the time-evolution of the RMSD profiles for C-alpha atoms of the protein and the ligand were determined and are shown in Figure 8.

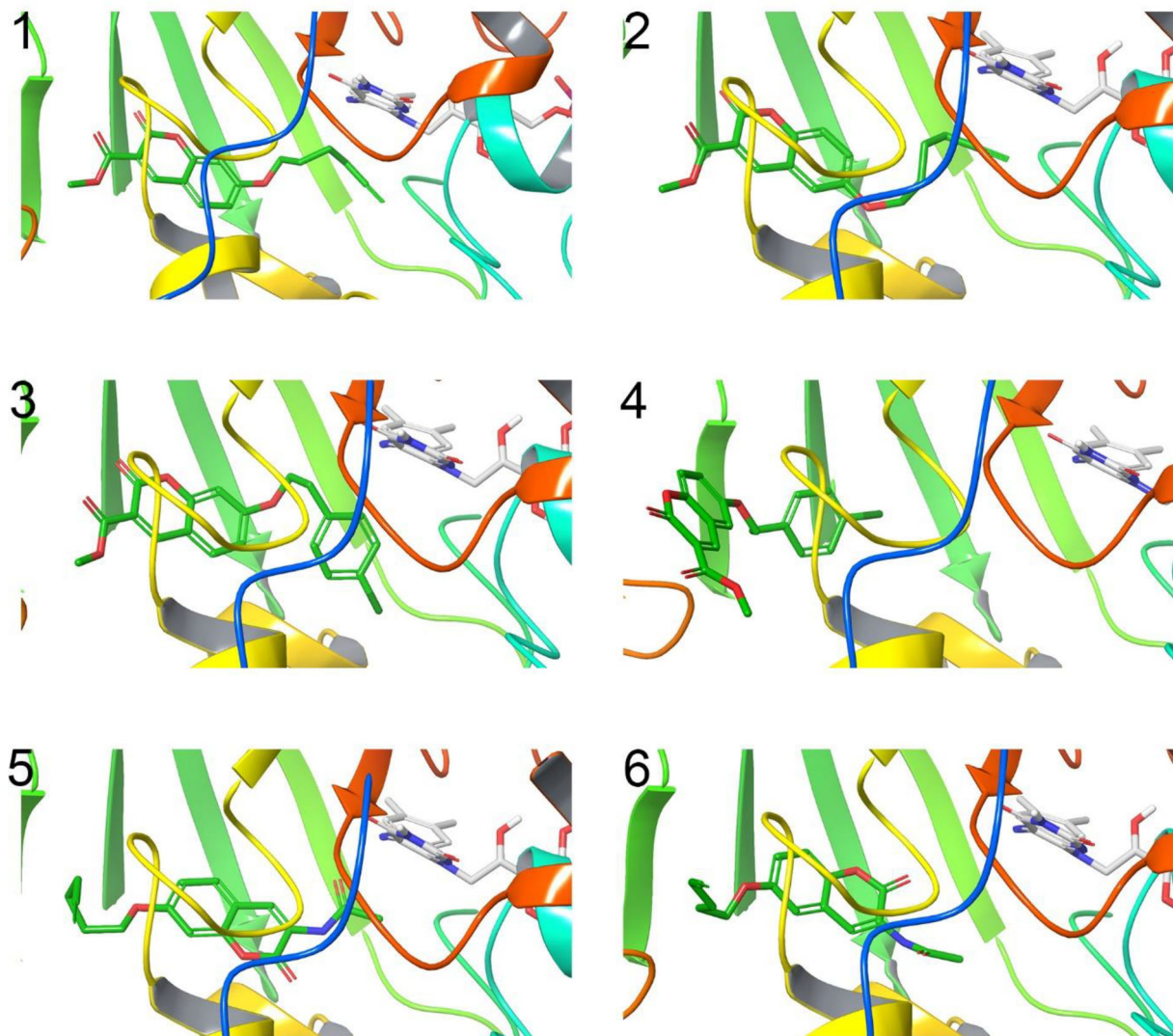
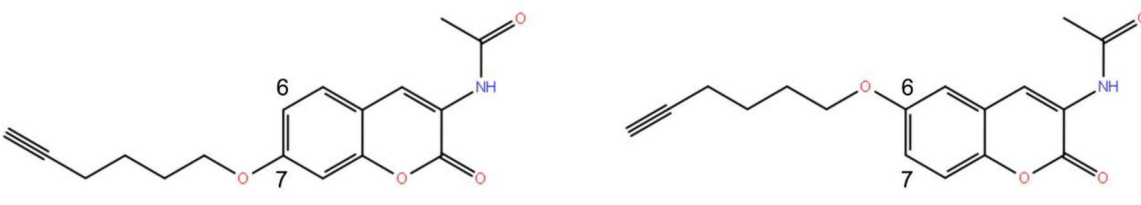


Figure 6. Docking poses of coumarin isomers with MAO-A active site. Binding conformations of coumarins are shown in green color, the C7-isomers are shown in 1,3,5 and their respective C6-isomers are shown in 2,4,6. FAD cofactor is shown in white color.



IC_{50} (MAO-A) = 66.8 nM
 IC_{50} (MAO-B) = 41.7 nM
SI (MAO-B) = 1.6

IC_{50} (MAO-A) > 10 000 nM
 IC_{50} (MAO-B) = 24.7 nM
SI (MAO-B) > 404

Figure 7. Chemical structures, IC_{50} values and selectivity index of the selected coumarins for MD simulation: C6-isomer (right) and C7-isomer (left).

The RMSD analysis of the C-alpha atoms of MAO-A and MAO-B in complex with C7-substituted coumarin displayed an increase in the RMSD for the first 20 ns up to 4.5 Å for MAO-A and 2.5 Å for MAO-B, whereas it remained stable with only small fluctuations averaging around 2.0 and 3.0 Å for the rest of the trajectory. On the other hand, the ligand RMSD seems to be stable in MAO-A for the MD simulation

duration and only fluctuates around 1.5 Å and 2.5 Å which is in the acceptable range. However, in MAO-B the ligand seems to reach higher RMSD values in the beginning of the simulation and peaks at 8 Å. However, it seems to be decreasing at the end of the trajectory which implies that the C7-isomer needed longer time to reach a stable state within the protein.

Table 4. ADME properties prediction results of the selected coumarin isomers.

Compound	QPlogS	%HOA	QPPCaco	QPlogBB	QPPMDCK	Rule of Five
1	-4.5	96.7	803.7	-1.0	390.6	0
2	-4.5	96.7	803.5	-1.0	390.5	0
3	-5.4	100.0	802.6	-0.7	961.3	0
4	-5.4	100.0	803.6	-0.7	962.6	0
5	-4.6	96.1	715.3	-1.1	344.4	0
6	-4.5	96.1	718.7	-1.1	346.2	0

QPlogS: Predicted aqueous solubility; %HOA: Percentage of human oral absorption; QPPCaco: Predicted apparent Caco-2 cell permeability; QPlogBB: Predicted brain/blood partition coefficient; QPPMDCK: Predicted apparent MDCK cell permeability; Rule of Three: Molecular weight (MW) \leq 500 g/mol; Number of hydrogen bond acceptors (HBA) \leq 10; Number of hydrogen bond donors (HBD) \leq 5; Number of rotatable bonds (nRotb) \leq 10 and lipophilicity clogPo/w \leq 5.

As for the C6-substituted coumarin, the RMSD analysis of MAO-A backbone shows a noticeable fluctuation in RMSD especially in the first 20 ns which reached 8 Å before starting to equilibrate after 39 ns around 6 Å for the rest of the simulation. The high deviation in backbone atoms of the protein could be linked to the bulky residue Phe-208 in MAO-A which doesn't allow the binding of long inhibitors, this could be more specific to the placement of the hex-5-ynoxy in position 6 of the coumarin scaffold which is directed towards the bottom of the cavity and might be constrained by the residue Phe-208. The corresponding C7-isomer was found to be more stable as the hex-5-ynoxy chain is more directed towards the flexible residue Ile-335 of the entrance cavity. For MAO-B, the backbone RMSD analysis shows a slight increase in RMSD in contrast with MAO-A which is stabilized around 3 Å, this difference in stability between the two

isoforms may well be due to the entrance cavity residues, the flexible Ile-199 residue in MAO-B better tolerate longer inhibitors to fit inside the substrate cavity by undergoing a conformational change which serves as a gate for MAO-B inhibitors.

On the other hand, ligand RMSD was calculated to indicate how stable the ligand is with respect to the protein and its active site cavity. The C6-substituted coumarin isomer in complex with MAO-A shows slight fluctuations around 3 Å. However, for MAO-B these fluctuations are less important as they average around 2.5 Å at the end of the trajectory.

The information obtained from the RMSD analysis could provide a clue into the dual inhibitory activity of the C7-isomer towards MAO-A and MAO-B when compared to the C6-isomer.

b) Root-mean square fluctuation (RMSF)

RMSF is useful for characterizing local changes along the protein chain. It is calculated from the motion of each residue around the average position along the trajectory revealing the flexibility of a certain region of the protein during the MD simulation. RMSF plots of the C-alpha atoms for the chosen complexes are shown in Figure 9.

The RMSF graphs indicate the flexibility and mobility of each amino acid throughout the simulation. Higher RMSF values imply greater flexibility during the MD simulation, whereas lower RMSF values interpret the good stability of the system. It is calculated from the motion of each residue around the average position along the trajectory revealing the flexibility of a certain region of the protein during the

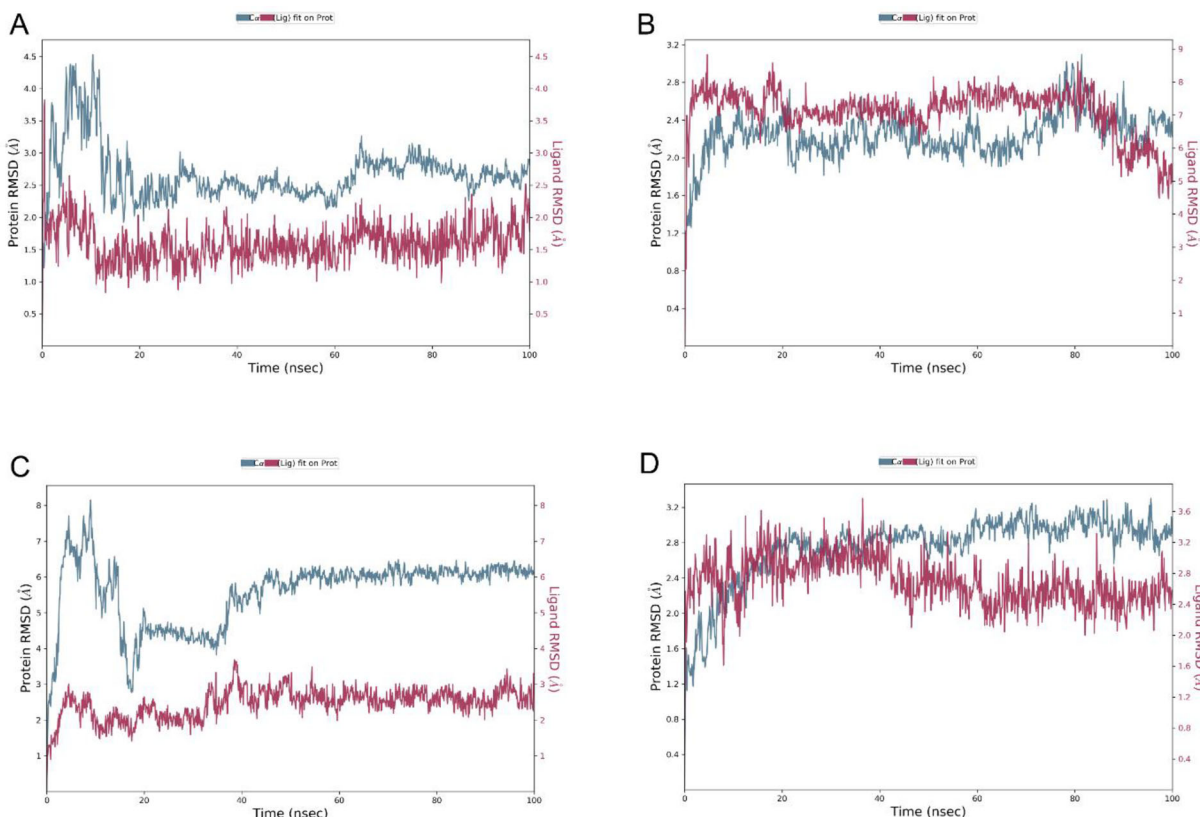


Figure 8. RMSD analysis of C-alpha atoms and ligand during MD simulation of C7-isomer with MAO-A (A) and MAO-B (B) and C6-isomer with MAO-A (C) and MAO-B (D).

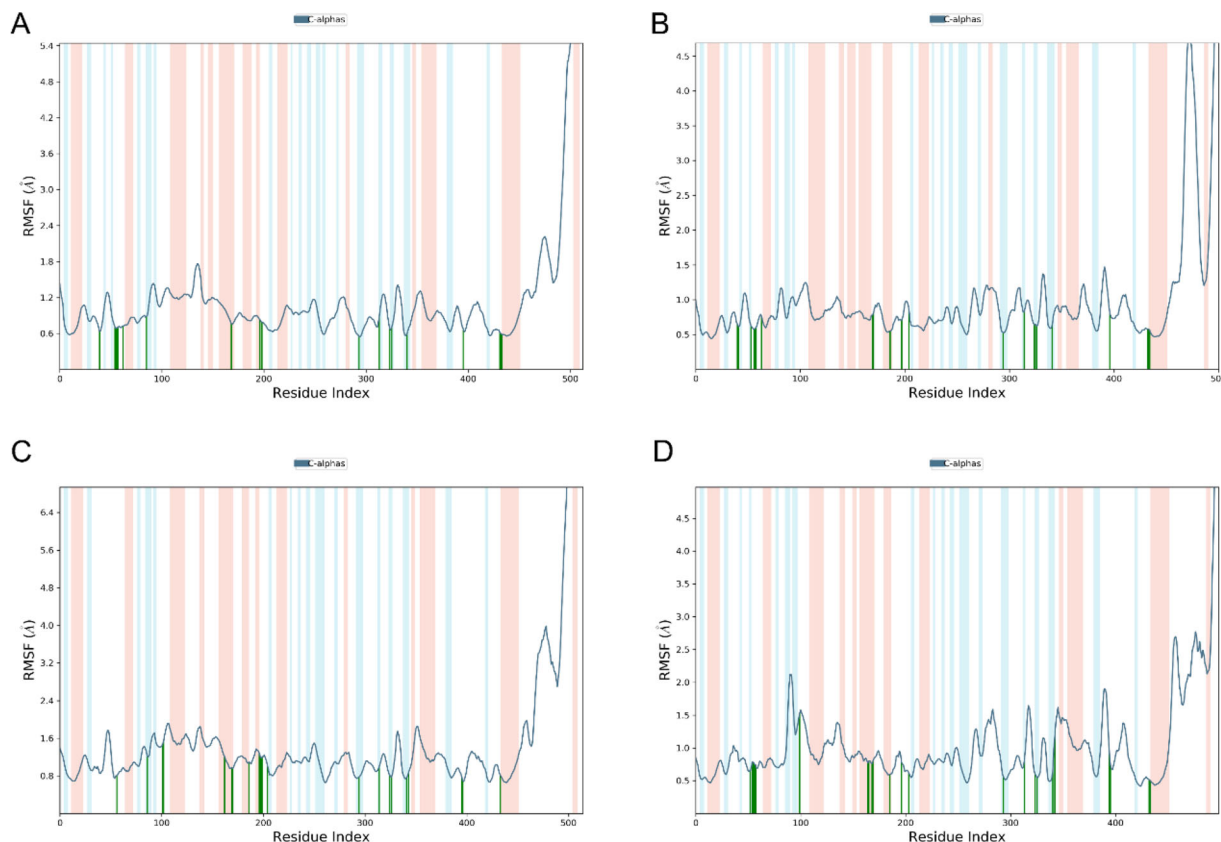


Figure 9. RMSF plots of C7-isomer with MAO-A (A) and MAO-B (B) and C6-isomer with MAO-A (C) and MAO-B (D) during MD simulation.

MD simulation. In this graph, the amino acids that make contacts with the ligand are represented by green vertical lines, secondary structural components such as α -helices and β -strands regions are represented by red and blue backgrounds, respectively, while the loop region is represented by a white background. Typically, α -helices and β -strands regions are rigid than the unstructured part of the protein, and hence fluctuate less than the loop regions. Compared to other parts of the protein, the N- and C-terminal regions showed the most fluctuations. The slight fluctuation of the active site and the main chain atoms indicates that the conformational change was minor (Martyna, 1994; Pawara et al., 2021; Zrieq et al., 2021). The RMSF graph of the C7-isomer and the C6-isomer with MAO-A and MAO-B enzymes complex yielded little fluctuations with less than 3 Å for residues in contact with ligands which is perfectly acceptable for small globular proteins (Vora et al., 2019).

c) Protein-ligand interactions analysis

Protein-ligand contacts were monitored throughout the simulation in order to clearly highlights the contribution of each residue of the binding site of each ligand-protein complex. The protein-ligand interactions diagrams are shown in Figure 10.

The C7-isomer was shown to establish a hydrogen bond with Tyr-69 of MAO-A and hydrophobic contacts mainly with Tyr-407 and Tyr-444 of the aromatic cage. Meanwhile the C7-isomer interacted with MAO-B through hydrogen bonding with Gly-434 and Met-436, stronger hydrophobic contacts

were observed between the ligand and Tyr-398 and Tyr-435 of the aromatic cage.

On the other hand, C6-isomer interacted with MAO-A through a hydrogen bond with Tyr-444, various hydrophobic interactions were noticed involving the residues: Ile-180, Phe-208, Ile-335, Phe-352 and Tyr-407. Meanwhile the C6-isomer in complex with MAO-B established three hydrogen bonds involving Ser-59, Tyr-60 and Gln-206, many hydrophobic contacts were observed with the residues: Tyr-389, Tyr-435, Phe-343, Tyr-326 and Ile-199. The results obtained from this analysis further emphasizes the role and implication of Ile-199 and Tyr-326 on shifting MAO-B selectivity as these two residues contribute largely in the binding of the C6-isomer to MAO-B in contrast with its respective C7-isomer.

d) MM-GBSA binding free energy calculations

The MD complexes were subjected to a post-MD MM-GBSA analysis in order to estimate their binding free energy. As noted in Table 5, among the four studied protein-ligand complexes, the C6-substituted coumarin in complex with MAO-B is showing the most negative value which indicates a stronger binding affinity (-71.05 kcal/mol), whereas it's estimated to -57.94 kcal/mol in the C7-isomer in complex with MAO-B which is in correlation with the experimental data. However, the large difference in potency for C6-isomer upon binding to MAO-A is not reflected in the GBSA binding free energy which suggests that certain residues in the binding pocket might suffer important rearrangements, which could have a conformational penalty not accounted for in the GBSA method.

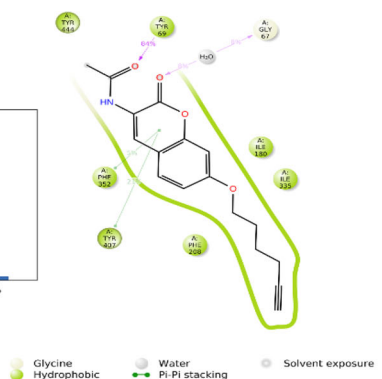
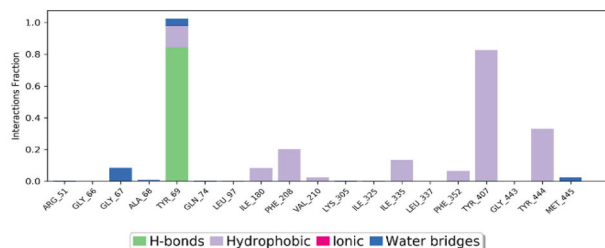
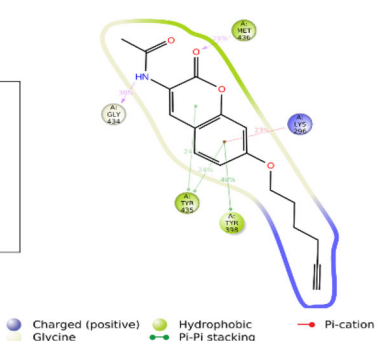
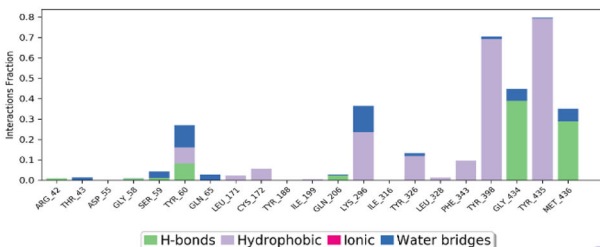
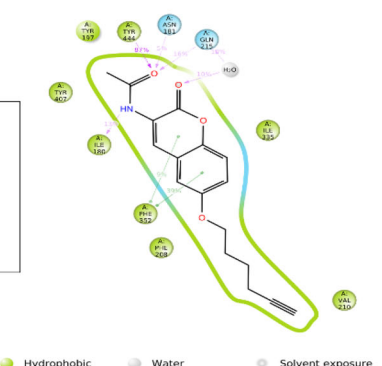
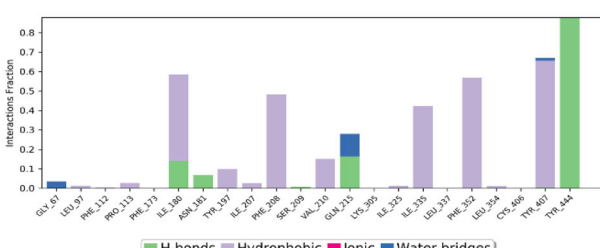
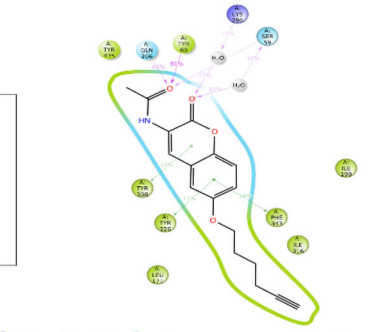
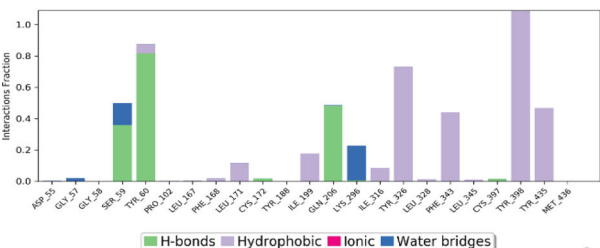
A**B****C****D**

Figure 10. Protein-ligand interactions diagrams and 2D representation of the C7-isomer with MAO-A (A) and MAO-B (B) and the C6-isomer with MAO-A (C) and MAO-B (D) throughout the MD simulation.

4. Discussion

Based on previously reported experimental data, it was confirmed that the C7-isomers of coumarins tend to be more potent towards MAO-B, meanwhile the C6-isomers are slightly less potent but tend to be more selective towards MAO-B isoform (Mertens et al., 2014). We noticed that this

hypothesis is applied to the selected coumarin derivatives: **1**, **3** and **5** and their respective C6-isomers: **2**, **4** and **6** which displayed a MAO-B selectivity shift of approximately 80, 80 and 400-fold respectively. Structural analysis revealed that the C6-substituted coumarin isomers form a π - π stacking interaction with Tyr-326 which is not present in the C7-substituted isomers.

Table 5. Post-MD MM-GBSA binding free energy results of C7-isomer with MAO-A (A) and MAO-B (B) and the C6-isomer with MAO-A (C) and MAO-B (D).

Protein-ligand complex	MM-GBSA binding free energy after MD (kcal/mol)
A	-59.63
B	-57.94
C	-69.95
D	-71.05

Furthermore, the positioning of the hex-5-ynyoxy moiety plays a role in the selectivity mechanism as the differences between MAO-A and MAO-B are mainly related to the shape and the flexibility of their active site cavities (Knez et al., 2020). The long and narrow cavity of MAO-B makes it preferentially bind long inhibitors which forces a conformational change of the gating residue Ile-199 and fuses the two cavities into one (Finberg & Rabey, 2016). The absence of this mechanism in MAO-A isoform further emphasize this hypothesis and could explain why such inhibitors tend to be more selective towards MAO-B.

Moreover, the molecular docking study confirmed that all coumarin derivatives bind non-covalently to MAO-B active site and the triple bond of the hex-5-ynyoxy chain doesn't bind to the FAD cofactor as such in irreversible inhibitors.

ADME properties prediction has shown that all the studied compounds are druglike, able to cross the blood-brain barrier and have values within recommended ranges where 95% of known drugs fall inside.

Lastly, a molecular dynamics simulation was conducted in order to assess and compare the stability of two coumarin isomers that displayed the highest selectivity shift towards MAO-B isoform (>404-fold). Analysis was conducted based on the RMSD of the protein backbone and ligands throughout the simulation, RMSF of the protein and protein-ligand interactions. The results showed favorable interactions and better stability regarding the C6-isomer with MAO-B isoform by establishing various hydrophobic interactions especially with Ile-199 and Tyr-326 which are known to play a role in substrate and inhibitors specificity (Edmondson et al., 2007). These residues are replaced with the bulky Phe-208 and Ile-335 in MAO-A which may hinder C6-substituted isomers from binding inside its active site cavity. Moreover, the selective C6-isomer was found to be unstable within MAO-A isoform in contrast to the non-selective C7-isomer which is in accordance with the experimental data.

5. Conclusion

The present study aimed to investigate the mode of interaction of previously reported alkynyl coumarinyl ethers at the molecular level. It was found that C7-isomers tend to be more potent towards MAO-A and MAO-B while the C6-isomers tend to be more selective towards MAO-B. Molecular docking analysis revealed that the loss of activity towards MAO-A of these compounds may be due to the bulky side chain of Phe-208 which is replaced by the gating residue Ile-199 that displays a conformational change depending on the nature of the inhibitor. Among the studied coumarin isomers, the compound **6** is considered the best drug-candidate

which needs more focus for the development of new anti-parkinsonian drugs in respect to its drug likeness, potency and selectivity for MAO-B. In conclusion, the computational investigation through molecular docking and molecular dynamics simulation helped elucidate not only the mechanism of MAO-B inhibition but also provide valuable insight for the rational improvements of selectivity of coumarin derivatives to be explored as novel drug candidates against Parkinson's disease.

Acknowledgments

We would like to thank Francisco Javier Luque Garriga, Professor in the Department of Chemical Physics, University of Barcelona, Spain, for his assistance. His contribution is sincerely appreciated and gratefully acknowledged.

Disclosure statement

No potential conflict of interest was reported by the authors.

Funding

The author(s) reported there is no funding associated with the work featured in this article.

ORCID

Yassir Boulaamane  <http://orcid.org/0000-0002-2939-7772>
 Iqrar Ahmad  <http://orcid.org/0000-0002-7697-9572>
 Harun Patel  <http://orcid.org/0000-0003-0920-1266>
 Niloy Das  <http://orcid.org/0000-0001-6848-3502>
 Mohammed Reda Britel  <http://orcid.org/0000-0002-9918-5767>
 Amal Maurady  <http://orcid.org/0000-0001-9298-717X>

References

- Ahmad, I., Jadhav, H., Shinde, Y., Jagtap, V., Girase, R., & Patel, H. (2021). Optimizing Bedaquiline for cardiotoxicity by structure based virtual screening, DFT analysis and molecular dynamic simulation studies to identify selective MDR-TB inhibitors. *In Silico Pharmacology*, 9(1), 23. <https://doi.org/10.1007/s40203-021-00086-x>
- Binda, C., Li, M., Hubálek, F., Restelli, N., Edmondson, D. E., & Mattevi, A. (2003). Insights into the mode of inhibition of human mitochondrial monoamine oxidase B from high-resolution crystal structures. *Proceedings of the National Academy of Sciences*, 100(17), 9750–9755. <https://doi.org/10.1073/pnas.1633804100>
- Binda, C., Mattevi, A., & Edmondson, D. E. (2011). Structural properties of human monoamine oxidases A and B. *International Review of Neurobiology*, 100, 1–11.
- Binda, C., Newton-Vinson, P., Hubálek, F., Edmondson, D. E., & Mattevi, A. (2002). Structure of human monoamine oxidase B, a drug target for the treatment of neurological disorders. *Nature Structural Biology*, 9(1), 22–26.
- Binda, C., Wang, J., Pisani, L., Caccia, C., Carotti, A., Salvati, P., Edmondson, D. E., & Mattevi, A. (2007). Structures of human monoamine oxidase B complexes with selective noncovalent inhibitors: Safinamide and coumarin analogs. *Journal of Medicinal Chemistry*, 50(23), 5848–5852.
- Congreve, M., Carr, R., Murray, C., & Jhoti, H. (2003). A rule of three for fragment-based lead discovery? *Drug Discovery Today*, 8(19), 876–877.
- Culpepper, L. (2013). Reducing the burden of difficult-to-treat major depressive disorder: Revisiting monoamine oxidase inhibitor therapy. *The Primary Care Companion for CNS Disorders*, 15(5), 27220. <https://doi.org/10.4088/PCC.13r01515>

- D. E. Shaw Research, Schrödinger Release. (2020–3). Desmond molecular dynamics system. Maestro-Desmond interoperability tools.
- Das, D., Koh, Y., Tojo, Y., Ghosh, A. K., & Mitsuya, H. (2009). Prediction of potency of protease inhibitors using free energy simulations with polarizable quantum mechanics-based ligand charges and a hybrid water model. *Journal of Chemical Information and Modeling*, 49(12), 2851–2862. <https://doi.org/10.1021/ci900320p>
- De Colibus, L., Li, M., Binda, C., Lustig, A., Edmondson, D. E., & Mattevi, A. (2005). Three-dimensional structure of human monoamine oxidase A (MAO A): Relation to the structures of rat MAO A and human MAO B. *Proceedings of the National Academy of Sciences*, 102(36), 12684–12689. <https://doi.org/10.1073/pnas.0505975102>
- Dorsey, E. R., Elbaz, A., Nichols, E., Abbasi, N., Abd-Allah, F., Abdelalim, A., Adsuar, J. C., Ansha, M. G., Brayne, C., Choi, J.-Y. J., Collado-Mateo, D., Dahodwala, N., Do, H. P., Edessa, D., Endres, M., Fereshtehnejad, S.-M., Foreman, K. J., Gankpe, F. G., Gupta, R., ... Murray, C. J. L. (2018). Global, regional, and national burden of Parkinson's disease, 199–2016: A systematic analysis for the Global Burden of Disease Study 2016. *The Lancet Neurology*, 17(11), 939–953. [https://doi.org/10.1016/S1474-4422\(18\)30295-3](https://doi.org/10.1016/S1474-4422(18)30295-3)
- Edmondson, D. E., Binda, C., & Mattevi, A. (2007). Structural insights into the mechanism of amine oxidation by monoamine oxidases A and B. *Archives of Biochemistry and Biophysics*, 464(2), 269–276. <https://doi.org/10.1016/j.abb.2007.05.006>
- Finberg, J. P., & Rabey, J. M. (2016). Inhibitors of MAO-A and MAO-B in psychiatry and neurology. *Frontiers in Pharmacology*, 7, 340.
- Friesner, R. A., Banks, J. L., Murphy, R. B., Halgren, T. A., Klicic, J. J., Mainz, D. T., Repasky, M. P., Knoll, E. H., Shelley, M., Perry, J. K., Shaw, D. E., Francis, P., & Sherk, P. S. (2004). Glide: A new approach for rapid, accurate docking and scoring. 1. Method and assessment of docking accuracy. *Journal of Medicinal Chemistry*, 47(7), 1739–1749.
- Friesner, R. A., Murphy, R. B., Repasky, M. P., Frye, L. L., Greenwood, J. R., Halgren, T. A., Sanschagrin, P. C., & Mainz, D. T. (2006). Extra precision glide: Docking and scoring incorporating a model of hydrophobic enclosure for protein–ligand complexes. *Journal of Medicinal Chemistry*, 49(21), 6177–6196. <https://doi.org/10.1021/jm051256o>
- Gaweska, H., & Fitzpatrick, P. F. (2011). Structures and mechanism of the monoamine oxidase family, 2(5), 365–377. <https://doi.org/10.1515/BMC.2011.030>
- Genheden, S., & Ryde, U. (2015). The MM/PBSA and MM/GBSA methods to estimate ligand-binding affinities. *Expert Opinion on Drug Discovery*, 10(5), 449–461. <https://doi.org/10.1517/17460441.2015.1032936>
- Greenwood, J. R., Calkins, D., Sullivan, A. P., & Shelley, J. C. (2010). Towards the comprehensive, rapid, and accurate prediction of the favorable tautomeric states of drug-like molecules in aqueous solution. *Journal of Computer-Aided Molecular Design*, 24(6–7), 591–604.
- Halgren, T. A., Murphy, R. B., Friesner, R. A., Beard, H. S., Frye, L. L., Pollard, W. T., & Banks, J. L. (2004). Glide: A new approach for rapid, accurate docking and scoring. 2. Enrichment factors in database screening. *Journal of Medicinal Chemistry*, 47(7), 1750–1759.
- Jacobson, M. P., Friesner, R. A., Xiang, Z., & Honig, B. (2002). On the role of the crystal environment in determining protein side-chain conformations. *Journal of Molecular Biology*, 320(3), 597–608.
- Jacobson, M. P., Pincus, D. L., Rapp, C. S., Day, T. J., Honig, B., Shaw, D. E., & Friesner, R. A. (2004). A hierarchical approach to all-atom protein loop prediction. *Proteins: Structure, Function, and Bioinformatics*, 55(2), 351–367. <https://doi.org/10.1002/prot.10613>
- Jorgensen, W. L., Maxwell, D. S., & Tirado-Rives, J. (1996). Development and testing of the OPLS all atom force field on conformational energetics and properties of organic liquids. *Journal of the American Chemical Society*, 118(45), 11225–11236. <https://doi.org/10.1021/ja9621760>
- Knez, D., Coletti, N., Iacovino, L. G., Sova, M., Pišlar, A., Konc, J., Lešnik, S., Higgs, J., Kamecki, F., Mangialavori, I., Dolšák, A., Žakelj, S., Trontelj, J., Kos, J., Binda, C., Marder, M., & Gobec, S. (2020). Stereoselective activity of 1-propargyl-4-styrylpiperidine-like analogues that can discriminate between monoamine oxidase isoforms A and B. *Journal of Medicinal Chemistry*, 63(3), 1361–1387. <https://doi.org/10.1021/acs.jmedchem.9b01886>
- Lee, H. Y., Cho, D. Y., Ahmad, I., Patel, H. M., Kim, M. J., Jung, J. G., Jeong, E. H., Haque, M. A., & Cho, K. M. (2021). Mining of a novel esterase (est3S) gene from a cow rumen metagenomic library with organophosphorus insecticides degrading capability: Catalytic insights by site directed mutations, docking, and molecular dynamic simulations. *International Journal of Biological Macromolecules*, 190, 441–455.
- Li, J., Abel, R., Zhu, K., Cao, Y., Zhao, S., & Friesner, R. A. (2011). The VSGB 2.0 model: A next generation energy model for high resolution protein structure modeling. *Proteins: Structure, Function, and Bioinformatics*, 79(10), 2794–2812. <https://doi.org/10.1002/prot.23106>
- Lin, J., Sahakian, D. C., De Morais, S. M., Xu, J. J., Polzer, R. J., & Winter, S. M. (2003). The role of absorption, distribution, metabolism, excretion and toxicity in drug discovery. *Current Topics in Medicinal Chemistry*, 3(10), 1125–1154.
- Lipinski, C. A. (2004). Lead- and drug-like compounds: The rule-of-five revolution. *Drug Discovery Today. Technologies*, 1(4), 337–341. <https://doi.org/10.1016/j.ddtec.2004.11.007>
- Lyne, P. D., Lamb, M. L., & Saeh, J. C. (2006). Accurate prediction of the relative potencies of members of a series of kinase inhibitors using molecular docking and MM-GBSA scoring. *Journal of Medicinal Chemistry*, 49(16), 4805–4808.
- Mallajosyla, J. K., Kaur, D., Chinta, S. J., Rajagopalan, S., Rane, A., Nicholls, D. G., Di Monte, D. A., MacArthur, H., & Andersen, J. K. (2008). MAO-B elevation in mouse brain astrocytes results in Parkinson's pathology. *PLoS ONE*, 3(2), e1616. <https://doi.org/10.1371/journal.pone.0001616>
- Martyna, G. J. (1994). Remarks on "Constant-temperature molecular dynamics with momentum conservation". *Physical Review. E, Statistical Physics, Plasmas, Fluids, and Related Interdisciplinary Topics*, 50(4), 3234–3236. <https://doi.org/10.1103/physreve.50.3234>
- Mehta, C. H., Narayan, R., Aithal, G., Pandiyan, S., Bhat, P., Dengale, S., Shah, A., Nayak, U. Y., & Garg, S. (2019). Molecular simulation driven experiment for formulation of fixed dose combination of Darunavir and Ritonavir as anti-HIV nanosuspension. *Journal of Molecular Liquids*, 293, 111469. <https://doi.org/10.1016/j.molliq.2019.111469>
- Mertens, M. D., Hinz, S., Müller, C. E., & Gütschow, M. (2014). Alkynyl-coumarin ethers as MAO-B inhibitors. *Bioorganic & Medicinal Chemistry*, 22(6), 1916–1928. <https://doi.org/10.1016/j.bmc.2014.01.046>
- Mostert, S., Petzer, A., & Petzer, J. P. (2015). Indanones as high-potency reversible inhibitors of monoamine oxidase. *ChemMedChem*, 10(5), 862–873. <https://doi.org/10.1002/cmdc.201500059>
- Noda, S., Sato, S., Fukuda, T., Tada, N., Uchiyama, Y., Tanaka, K., & Hattori, N. (2020). Loss of Parkin contributes to mitochondrial turnover and dopaminergic neuronal loss in aged mice. *Neurobiology of Disease*, 136, 104717. <https://doi.org/10.1016/j.nbd.2019.104717>
- Olsson, M. H., Søndergaard, C. R., Rostkowski, M., & Jensen, J. H. (2011). PROPKA3: Consistent treatment of internal and surface residues in empirical pK_a predictions. *Journal of Chemical Theory and Computation*, 7(2), 525–537. <https://doi.org/10.1021/ct100578z>
- Pawara, R., Ahmad, I., Surana, S., & Patel, H. (2021). Computational identification of 2,4-disubstituted amino-pyrimidines as L858R/T790M-EGFR double mutant inhibitors using pharmacophore mapping, molecular docking, binding free energy calculation, DFT study and molecular dynamic simulation. *In Silico Pharmacol*, 9 (1), 54. <https://doi.org/10.1007/s40203-021-00113-x>
- Poewe, W., & Mahlknecht, P. (2020). Pharmacologic treatment of motor symptoms associated with Parkinson disease. *Neurologic Clinics*, 38(2), 255–267. <https://doi.org/10.1016/j.ncl.2019.12.002>
- Rempel, V., Volz, N., Hinz, S., Karcz, T., Meliciani, I., Nieger, M., Wenzel, W., Bräse, S., & Müller, C. E. (2012). 7-Alkyl-3-benzylcoumarins: A versatile scaffold for the development of potent and selective cannabinoid receptor agonists and antagonists. *Journal of Medicinal Chemistry*, 55(18), 7967–7977.
- Roos, K., Wu, C., Damm, W., Reboul, M., Stevenson, J. M., Lu, C., Dahlgren, M. K., Mondal, S., Chen, W., Wang, L., Abel, R., Friesner, R. A., & Harder, E. D. (2019). OPLS3e: Extending force field coverage for drug-like small molecules. *Journal of Chemical Theory and Computation*, 15(3), 1863–1874. <https://doi.org/10.1021/acs.jctc.8b01026>
- Schrödinger Release: Maestro. (2021). Schrödinger, LLC.
- Shih, J. C., Chen, K., & Ridd, M. J. (1999). Monoamine oxidase: From genes to behavior. *Annual Review of Neuroscience*, 22(1), 197–217.

- Son, S. Y., Ma, J., Kondou, Y., Yoshimura, M., Yamashita, E., & Tsukihara, T. (2008). Structure of human monoamine oxidase A at 2.2-Å resolution: The control of opening the entry for substrates/inhibitors. *Proceedings of the National Academy of Sciences*, 105(15), 5739–5744. <https://doi.org/10.1073/pnas.0710626105>
- Tetrud, J. W., & Koller, W. C. (2004). A novel formulation of selegiline for the treatment of Parkinson's disease. *Neurology*, 63(7 Suppl 2), S2–S6. suppl
- Vora, J., Patel, S., Athar, M., Sinha, S., Chhabria, M. T., Jha, P. C., & Shrivastava, N. (2019). Pharmacophore modeling, molecular docking and molecular dynamics simulation for screening and identifying anti-dengue phytocompounds. *Journal of Biomolecular Structure and Dynamics*, 38(6), 1726–1740. <https://doi.org/10.1080/07391102.2019.1615002>
- Wang, D., Hong, R. Y., Guo, M., Liu, Y., Chen, N., Li, X., & Kong, D. X. (2019). Novel C7-substituted coumarins as selective monoamine oxidase inhibitors: Discovery, synthesis and theoretical simulation. *Molecules*, 24(21), 4003. <https://doi.org/10.3390/molecules24214003>
- Youdim, M. B., Gross, A., & Finberg, J. P. (2001). Rasagiline [N-propargyl-1R (+)-aminoindan], a selective and potent inhibitor of mitochondrial monoamine oxidase B. *British Journal of Pharmacology*, 132(2), 500–506.
- Youdim, M. B., Edmondson, D., & Tipton, K. F. (2006). The therapeutic potential of monoamine oxidase inhibitors. *Nature Reviews. Neuroscience*, 7(4), 295–309.
- Zrieq, R., Ahmad, I., Snoussi, M., Noumi, E., Iriti, M., Algahtani, F. D., Patel, H., Saeed, M., Tasleem, M., Sulaiman, S., Aouadi, K., & Kadri, A. (2021). Tomatidine and Patchouli alcohol as inhibitors of SARS-CoV-2 enzymes (3CLpro, PLpro and NSP15) by molecular docking and molecular dynamics simulations. *International Journal of Molecular Sciences*, 22(19), 10693. <https://doi.org/10.3390/ijms221910693>